Acta Crystallographica Section D
Biological Crystallography
ISSN 0907-4449

Structural and functional characterization of *Mycobacterium tuberculosis* triosephosphate isomerase

Sean E. Connor, Glenn C. Capodagli, Michelle K. Deaton and Scott D. Pegan*

Department of Chemistry and Biochemistry, University of Denver, Denver, USA

Correspondence e-mail: spegan@du.edu

Received 10 August 2011
Accepted 17 October 2011

PDB References: triosephosphate isomerase, apo, 3ta6; phosphoglycolohydroxamate complex, 3tao.

Tuberculosis (TB) is a major infectious disease that accounts for over 1.7 million deaths every year. *Mycobacterium tuberculosis*, the causative agent of tuberculosis, enters the human host by the inhalation of infectious aerosols. Additionally, one third of the world's population is likely to be infected with latent TB. The incidence of TB is on the rise owing in part to the emergence of multidrug-resistant strains. As a result, there is a growing need to focus on novel *M. tuberculosis* enzyme targets. *M. tuberculosis* triosephosphate isomerase (MtTPI) is an essential enzyme for gluconeogenetic pathways, making it a potential target for future therapeutics. In order to determine its structure, the X-ray crystal structure of MtTPI has been determined, as well as that of MtTPI bound with a reaction-intermediate analog. As a result, two forms of the active site were revealed. In conjunction with the kinetic parameters obtained for the MtTPI-facilitated conversion of dihydroxyacetone phosphate (DHAP) to D-glyceraldehyde-3-phosphate (D-GAP), this provides a greater structural and biochemical understanding of this enzyme. Additionally, isothermal titration calorimetry was used to determine the binding constant for a reaction-intermediate analog bound to the active site of MtTPI.

1. Introduction

Tuberculosis (TB) is one of the most prevalent infections in the world and is a leading cause of mortality in developing countries. The World Health Organization estimates that 9.4 million new cases of infection by *Mycobacterium tuberculosis*, the causative agent of TB, were reported in 2009. Additionally, the World Health Organization estimates that more than one in three people possess the latent form of TB (World Health Organization, 2010). Furthermore, incidences of multidrug-resistant TB and extensive drug-resistant TB are on the rise, requiring the development of new treatment regimens, drugs and drug targets (World Health Organization, 2008).

One potential drug target for *M. tuberculosis* is the glycolytic enzyme triosephosphate isomerase (MtTPI). MtTPI is a key enzyme in the Embden–Meyerhof pathway, interconverting dihydroxyacetone phosphate (DHAP) and D-glyceraldehyde-3-phosphate (D-GAP) (Fig. 1). In glycolysis MtTPI utilizes these two products for the formation of two pyruvate molecules, while in gluconeogenesis MtTPI ensures that both substrates are produced for fructose-1,6-bisphosphate aldolase (FBA) to synthesize fructose 1,6-bisphosphate (FBP; Mathur *et al.*, 2006). Therefore, MtTPI is crucial for the supply of these precursor molecules necessary for other biochemical

pathways that are essential for the survival of *M. tuberculosis*. In general, triosephosphate isomerases (TPIs, also known as TIMs) are homodimers with 25–27 kDa subunits; each subunit consists of a single eight-stranded α/β-barrel domain (Wierenga, 2001; Wierenga *et al.*, 2010). TPI is a highly conserved enzyme, with *M. tuberculosis* TPI having 40% similarity to *Escherichia coli* TPI (Fig. 2). A characteristic structural feature of triosephosphate isomerases is flexibility of loops 6 and 7, which are shown in parentheses in Fig. 2. Movement of these loops constitutes a change from an open unbound conformation to a closed bound conformation (Kempf *et al.*, 2007; Wang *et al.*, 2009).

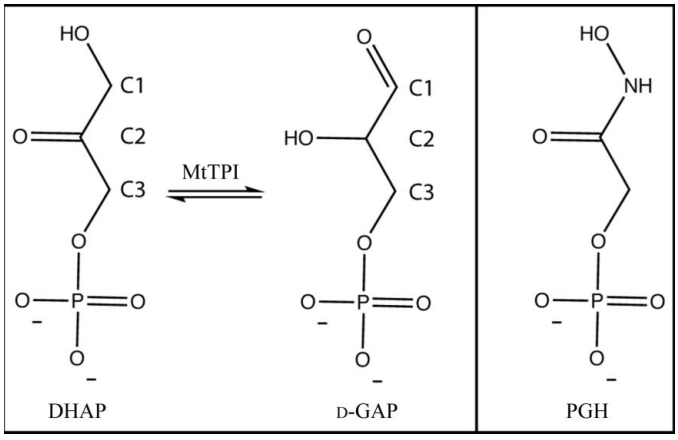

Figure 1
Exchange between DHAP and D-GAP *via* MtTPI. Left, TPI catalyzes the exchange of DHAP and D-GAP. PGH is a reaction-intermediate analog. Right, chemical structure of the reaction-intermediate analog phosphoglycolohydroxamate (PGH).

Recently, the X-ray structure of MtTPI with glycerol bound in its active site (MtTPI–GOL) was released in the PDB. This structure may represent the substrate-bound form of the enzyme, the apo form or neither. In order to gain further insight into this, X-ray structures of MtTPI in its apo form and bound to a reaction-intermediate analog were determined to high resolution in the absence of glycerol. They revealed significant conformational change in active-site loops 6 and 7 of MtTPI when bound to a reaction-intermediate analog. Additionally, isothermal titration calorimetry (ITC) was used to determine the binding constants for the complex of MtTPI with phosphoglycolohydroxamate (MtTPI–PGH) and kinetic assays were performed to determine the K_m and k_{cat} for the conversion of DHAP to D-GAP.

2. Methods and materials

The *M. tuberculosis* TPI gene (*tpiA*) was PCR-amplified from *M. tuberculosis* H37Rv genomic DNA using the oligonucleotides 5′-GGAATTC**CATATG**AGCCGCAAGCCGCTGATAG-3′ and 3′-CAA**CTCGAG**CGGCAACGGACCACCGGCCG-5′ as the forward primer and the reverse primer, respectively. *Nde*I and *Xho*I restriction sites (in bold) were incorporated into the primers for cloning into the expression vector pET-24b harboring the MtTPI gene (pET-TPI). The pET-TPI construct was heat-shock transformed into *E. coli* BL21 (DE3) cells and grown at 310 K in 1.5 l LB broth containing 50 µg ml^{-1} kanamycin until the OD_{600} reached 0.6. The cells were induced with 1 m*M* IPTG for 4–6 h at 298 K and then harvested *via* centrifugation at 3000*g* for 10 min. The cell pellet was suspended in 200 ml buffer *A* (50 m*M* sodium/

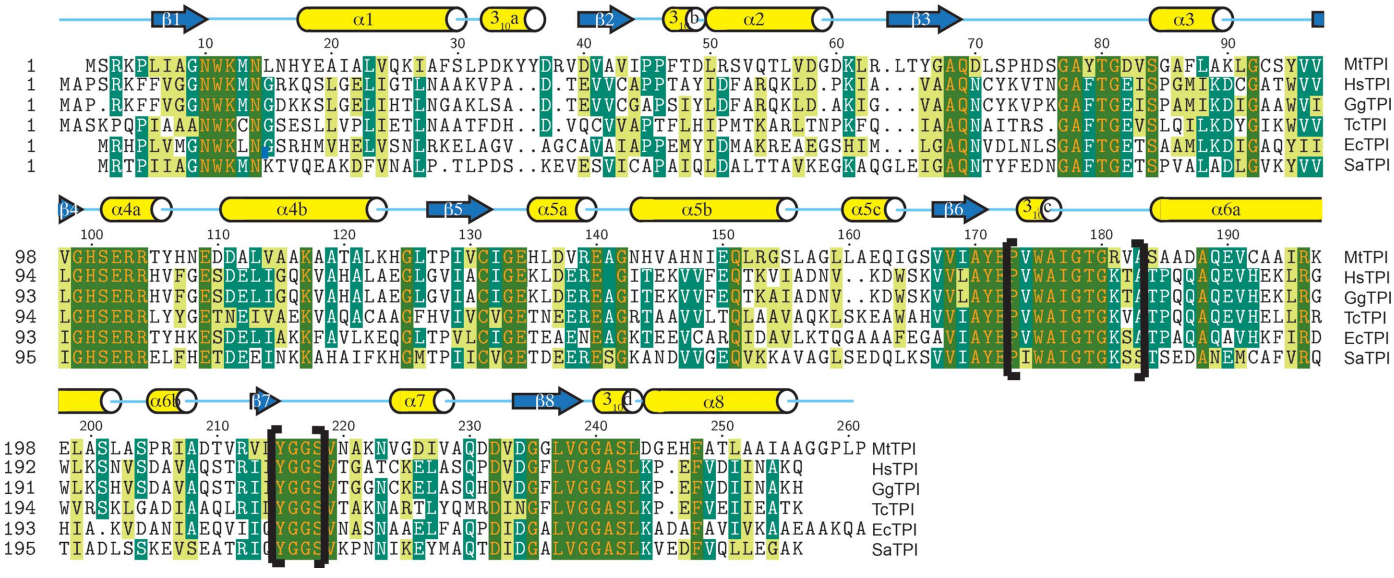

Figure 2
Sequence alignment of the monomeric chains of MTPI and five TPI homologs. Loops 6 and 7 are shown in parentheses. The secondary-structure elements from MtTPI are shown above the alignment as predicted by *DSSP*. The sequences are ordered from lowest to highest similarity to MtTPI (from top to bottom). Accordingly, TPI from *Homo sapiens* (HsTPI; gi_1200507) is 37% similar, TPI from *Gallus gallus* (GgTPI; gi_45382061) is 37% similar, TPI from *Trypanosoma cruzi* strain CL Brener (TcTPI; gi_71662494) is 38% similar, TPI from *E. coli* (EcTPI; gi_89110110) is 40% similar and TPI from *Staphylococcus aureus* subsp. *aureus* MW2 (SaTPI; gi_21282465) is 42% similar. Alignment and similarity calculations were obtained using *ClustalW* and *TEXshade* programs from http://workbench.sdsc.edu.

Table 1
Data-collection and refinement statistics for MtTPI.

Values in parentheses are for the last resolution shell.

	MtTPI–PGH	MtTPI–APO
Data collection		
Space group	*C*2	*C*2
Unit-cell parameters (Å, °)	a = 134.0, b = 55.7, c = 76.9, $\alpha = \gamma = 90$, $\beta = 104.03$	a = 134.9, b = 52.6, c = 77.5, $\alpha = \gamma = 90$, $\beta = 104.5$
Resolution (Å)	74.65–1.45	75.07–1.41
No. of reflections observed	397311	413043
No. of unique reflections	94064	100458
$R_{\rm merge}$† (%)	4.3 (18.8)	4.0 (22.9)
$\langle I/\sigma(I)\rangle$	41.5 (6.2)	38.7 (4.6)
Completeness (%)	96.4	99.1
Refinement		
Resolution range	74.65–1.45	75.07–1.41
No. of reflections in working set	89362	95369
No. of reflections in test set	4702	5003
$R_{\rm work}$‡ (%)	16.1	13.1
$R_{\rm free}$‡ (%)	18.3	15.5
Mean B factor (Å^2)	16.7	17.0
Protein B factor (Å^2)	13.8	12.7
Water B factor (Å^2)	29.3	31
Ligand B factor (Å^2)	20.5	18.6
Occupancy of ligand (site 1/site 2)§ (%)	70.0/50.0	100.0
R.m.s. deviations		
Bond lengths (Å)	0.01	0.01
Bond angles (°)	1.30	1.17
Protein atoms	4103	3989
Water atoms	844	827
Monomers in asymmetric unit	2	2

† $R_{\rm merge} = \sum_{hkl}\sum_i |I_i(hkl) - \langle I(hkl)\rangle|/\sum_{hkl}\sum_i I_i(hkl)$, where $I_i(hkl)$ is the ith measurement and $\langle I(hkl)\rangle$ is the weighted mean of all measurements of $I(hkl)$. ‡ $R_{\rm work}$ and $R_{\rm free} = \sum_{hkl} ||F_{\rm obs}| - |F_{\rm calc}||/\sum_{hkl}|F_{\rm obs}|$ for reflections in the working and test sets, respectively. § Occupancy of PGH within the two active sites of MtTPI–PGH and the one citrate anion found bound to MtTPI–APO.

potassium phosphate pH 8.0, 300 m*M* NaCl) with 5 mg lysozyme (Fisher Scientific). The cells were then sonicated on ice using an ultrasonic dismembrator (Model 150E, Fisher Scientific) at 30% power with 5 s pulses for 10 min. Insoluble cell debris was removed by centrifugation at 23 000*g* for 45 min at 277 K. The supernatant was filtered using 0.8 µm Whatman Nylon Membrane filters and loaded onto Ni–NTA His-Bind resin (Novagen) pre-equilibrated in buffer *A*. MtTPI bound to the column was then washed with five column volumes of buffer *A* plus 10 m*M* imidazole. MtTPI was then eluted from the column using five column volumes of buffer *A* plus 250 m*M* imidazole. The eluate was loaded onto a Superdex 200 HK HiLoad 26/60 FPLC column pre-equilibrated with buffer *B* (5 m*M* HEPES pH 7.4, 2 m*M* DTT, 50 m*M* NaCl) and eluted at a flow rate of 1.5 ml min^{-1}. Fractions were pooled according to the chromatogram, concentrated to 10 mg ml^{-1} in a Vivaspin 20 (GE) centrifuge concentrator and filtered through a 0.65 µm membrane filter. All protein concentrations were determined from the absorbance at 280 nm (Gill & von Hippel, 1989).

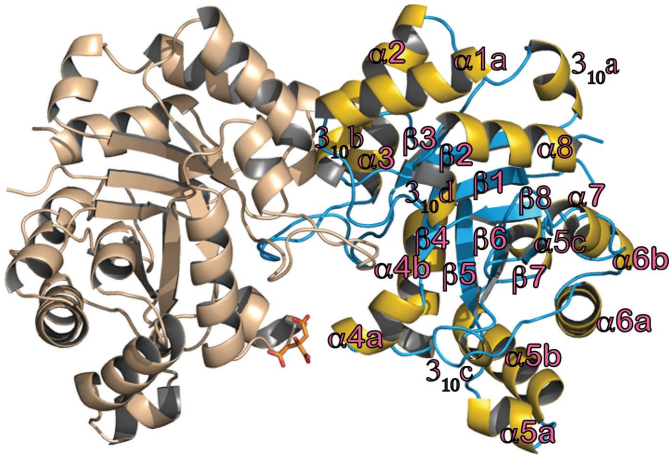

Figure 3
Cartoon representation of apo MtTPI. The *B* monomer is colored tan, while the helical regions of the *A* monomer are rendered in yellow with β-strands and loops in blue. The citrate anion is illustrated in stick form with its C atoms colored orange and O atoms colored red. Labels for monomer *A* are shown in pink.

Initial crystallization conditions for MtTPI were obtained from the MtTPI–GOL structure deposited in the RCSB (PDB entry 3gvg; Seattle Structural Genomics Center for Infectious Disease, unpublished work). Using these conditions as a guide, a gradient of 10–20% PEG 3350 and 100–250 m*M* ammonium citrate was used for initial screening. Analysis of these conditions revealed that crystal formation was improved at higher ammonium citrate concentrations (250 m*M*) and a PEG 3350 concentration of 16%. Final crystals were obtained by vapor diffusion using 4 µl drops equilibrated over 500 µl reservoir solution. Hanging drops were formed by mixing the protein solution in a 1:1 ratio with a precipitant solution consisting of 250 m*M* ammonium citrate and 16% PEG 3350. MtTPI–PGH complex crystals were sourced from MtTPI–APO crystals soaked in mother liquor containing 2 m*M* PGH for 24 h. X-ray diffraction data were collected for both MtTPI crystals on the LS-CAT beamline at the Advanced Photon Source (APS), Argonne National Laboratory. Crystals were mounted on nylon loops and submerged in a 4 µl drop of well solution. The crystals were immediately flash-cooled by submersion in liquid nitrogen. Frozen crystals were mounted on a goniostat under a stream of dry N_2 at 100 K. X-ray exposures of 1 s per degree of rotation over a total of 200° in φ at 0.978 Å were collected on a MAR 300 CCD for all crystals. X-ray images were processed and scaled using *HKL*-2000 (Otwinowski & Minor, 1997). Molecular-replacement solutions were derived using *Phaser* with MtTPI–GOL (PDB entry 3gvg) as the search model (McCoy *et al.*, 2007). *WinCoot* was used for model building and *REFMAC*5.5 from the *CCP*4 suite was used for refinement (Winn *et al.*, 2011; Emsley & Cowtan, 2004). Coordinates and molecular-library files for the ligands PGH and citrate were built using the *CCP*4 suite

program *SKETCHER*. Anisotropic temperature factors were used in the refinement of the MtTPI–APO and MtTPI–PGH structures. Water molecules were added to $F_o - F_c$ density peaks that were greater than 3σ using the 'Find Water' function in *WinCoot*. The final models were checked for structural quality using the *CCP*4 suite programs *PROCHECK* and *SFCHECK*. Structure factors and final coordinates have been deposited in the Protein Data Bank and were assigned codes 3ta6 (MtTPI–APO) and 3tao (MtTPI–PGH). Data-collection and refinement statistics are given in Table 1.

K_m and k_{cat} were determined enzymatically in triplicate. The activity of MtTPI was coupled to rabbit glyceraldehyde phosphate dehydrogenase (GAPDH), which reduces NAD^+ to NADH during the conversion of D-GAP to glycerate 1,3-bisphosphate. The formation of NADH was monitored through the absorption by NADH at 340 nm using a SpectraMax Plus 384 plate reader. The reaction wells contained 0.4 m*M* NAD^+, 2.0 U ml^{-1} rabbit GAPDH, 0.02% BSA, 15 m*M* potassium dihydrogen arsenate, 100 m*M* potassium acetate, 100 m*M* Tris pH 7.8 and 200 n*M* MtTPI. To determine the kinetic constants, the initial velocity data were fitted to the Michaelis–Menten equation, $\upsilon = V_{max}/\{1 + (K_m/[S])\}$, using the *Enzyme Kinetics Module* 1.3 of *Sigma Plot* v.10 (SPSS Inc.). The k_{cat} value was calculated from V_{max} and the enzyme concentration $[E]$ *via* the equation $k_{cat} = V_{max}/[E]$.

Isothermal titration calorimetry (ITC) experiments were conducted using a Nano ITC system (TA Instruments, Utah, USA). MtTPI was dialyzed overnight against a solution consisting of 5 m*M* HEPES pH 7.4, 100 m*M* NaCl, 2 m*M* DTT. PGH was brought to a concentration of 2.5 m*M* using the buffer in which MtTPI was dialyzed. ITC runs of MtTPI and PGH were performed in duplicate and comprised of 25 2 µl injections of 2.5 m*M* PGH into 0.343 m*M* MtTPI. Each injection was spaced 200 s apart. The average heat released for the last five injections was used to correct for the heat of dilution. Data sets were analyzed with *NanoAnalyze* software and fitted to an independent model.

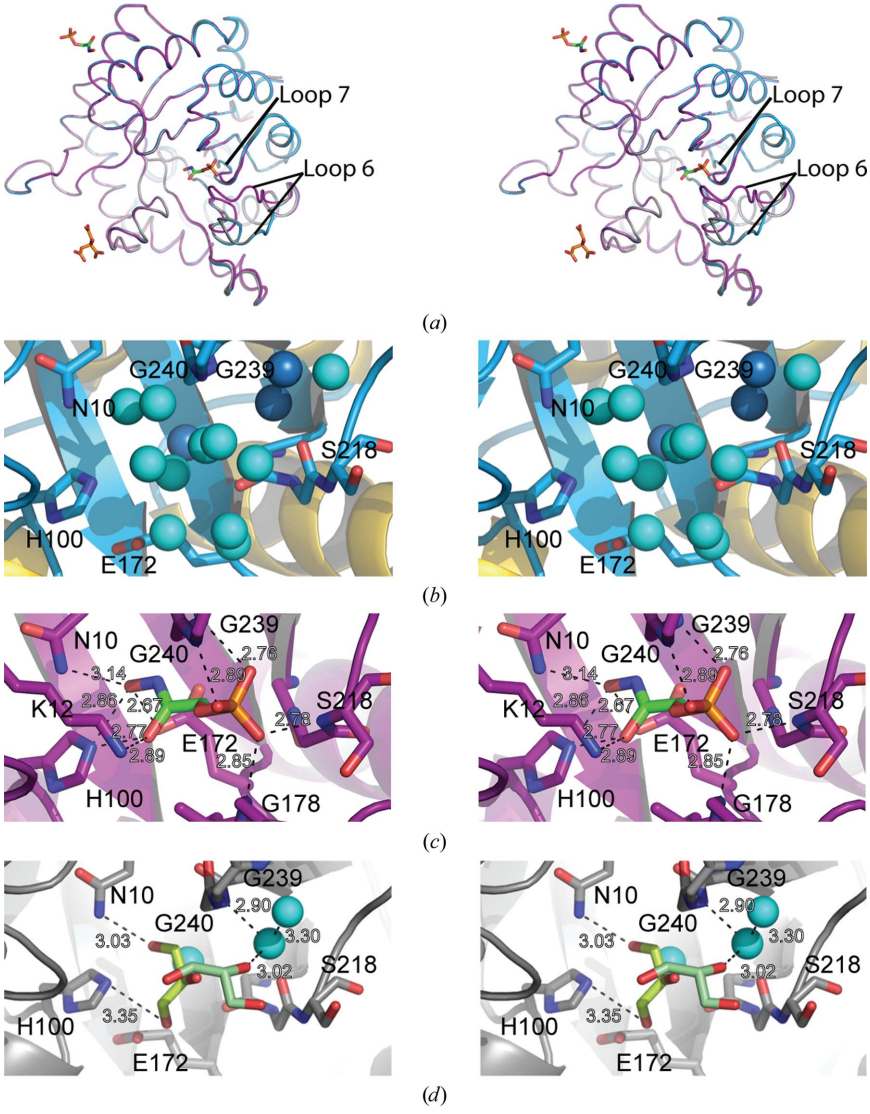

Figure 4
Active site of MtTPI in apo, PGH-bound and glycerol-bound states. (*a*) Wall-eyed stereoview of secondary-structure matching alignment of MtTPI–APO (blue), MtTPI–PGH (lavender) and MtTPI–GOL (gray; PDB entry 3gvg). The citrate bound to MtTPI–APO is rendered as sticks in orange, while PGH from MtTPI–PGH is rendered as sticks in green. (*b*) Wall-eyed stereoview of the MtTPI–APO active site located in monomer *A*. MtTPI is rendered in cartoon representation and colored according to secondary structure, with loops and β-sheets in blue and α-helices in yellow. All waters are depicted as spheres. Three active-site-located waters present in both MtTPI–APO and MtTPI–GOL are colored sky blue. The remaining waters are colored cyan. (*c*) Wall-eyed stereoview of the MtTPI–PGH active site located in monomer *A*. MtTPI is rendered in cartoon representation and colored according to secondary structure, with loops, β-sheets and α-helices in lavender. PGH is depicted in sticks and colored green. (*d*) MtTPI is rendered in cartoon representation and colored according to secondary structure, with loops, β-sheets and α-helices in gray. Glycerol is depicted in stick representation and colored green with red O atoms.

3. Results and discussion

In order to determine the structure of MtTPI in the absence of glycerol, MtTPI was expressed and purified without the use of glycerol. The protein was concentrated to 10 mg ml^{-1} (360 µ*M*). The protein was then screened using similar crystallization conditions to those of MtTPI–GOL (PDB entry 3gvg). Optimization of the conditions using a mixture of a lower PEG 3350 concentration and higher ammonium citrate concentrations produced crystals that diffracted to 1.41 Å resolution. The X-ray structure was subsequently solved in space group *C*2 by molecular replacement using the MtTPI–GOL structure (PDB entry 3gvg) as a search model. MtTPI was found to have a dimer in

the asymmetric unit. As in other known TPI structures, the secondary structure of MtTPI is comprised of 12 α-helices, four 3_{10}-helices and eight β-sheets (Fig. 3). Intriguingly, the X-ray structure of MtTPI–APO closely resembles the MtTPI–GOL structure in terms of both secondary and tertiary structure, suggesting that the MtTPI–GOL structure represents the apo form of the enzyme (Fig. 4). Additionally, a closer comparison of the MtTPI–GOL and MtTPI–APO active sites reveals that water occupies the space of the glycerol in the MtTPI structure (Figs. 4*b* and 4*c*).

In order to determine the nature of any structural changes that occur during MtTPI catalysis, attempts were made to soak MtTPI crystals and cocrystallize MtTPI using DHAP concentrations of up to 2 m*M*. However, despite using DHAP concentrations approximately five times that of the enzyme, no density attributed to DHAP was found within crystals generated under these circumstances; instead, they reflected the MtTPI–APO structure. Phosphoglycolohydroxamate (PGH) was then used as an intermediate analog. PGH is similar to DHAP, with the exchange of a C atom for an N atom (Fig. 1). The enzymatic reaction for the conversion of DHAP to D-GAP proceeds through an enediolate intermediate structure, of which PGH is an analog. PGH has been used previously as a reaction-intermediate analog of DHAP (Davenport *et al.*, 1991; Pegan *et al.*, 2009; Serratos *et al.*, 2011). PGH was obtained from Dr Olga Krasnykh at the Institute for Tuberculosis Research, the University of Illinois at Chicago. It was synthesized according to a previously established protocol (Pegan *et al.*, 2009). MtTPI crystals were soaked in 2 m*M* PGH for 24 h and this resulted in the crystal structure of a substrate-bound form of the enzyme. Comparison of MtTPI–PGH to MtTPI–APO revealed significant conformational changes in the regions of loops 6 and 7 of monomer *A* (Fig. 4*a*). Flexibility of loops 6 and 7 has been noted in other triosphosphate isomerases as key to hydrogen bonding the phosphate moiety of the substrate (Berlow *et al.*, 2007; Wang *et al.*, 2009). Comparison of the tertiary structures of MtTPI–PGH and MtTPI–GOL reveals a shift in loop 6 of 7.34 Å and a smaller 0.55 Å shift in loop 7. Closer inspection of the active site of monomer *A* reveals a significant peak in $F_o - F_c$ electron-density difference maps. Modeling of PGH at 70% occupancy in the chain *A* active site completely accounts for this density. Density accounting for an additional PGH was also located on the periphery of chain *A*. Interestingly, no similar density for PGH was observed in the chain *B* active site. The position of PGH in the chain *A* active site allows hydrogen-bonding interactions between the O atoms of the phosphate dianion group and Gly239, Gly240, Gly178 and Ser218 of MtTPI that range from 2.76 to 2.89 Å. It has been proposed by Wierenga *et al.* (2010) that the closing of these loops 6 and 7 generates a phosphate dianion-binding pocket, in which the phosphate dianion moiety is secured by four hydrogen bonds to four main-chain NH groups of loops 6, 7 and 8. The geometry of the four NH groups in loops 6–8 provides a more favorable binding site for dianion phosphates in comparison to monoanion analogs, which bind with low affinity (Belasco *et al.*, 1978; Wierenga *et al.*, 2010). This binding of the phosphate group may prevent undesired phosphate elimination during the reaction, as observed in noncatalyzed free three-carbon sugar phosphates in solution (Wierenga *et al.*, 2010). As seen in other TPIs, the conformational changes of loops 6 and 7 correspond to a large shift in the catalytic base Glu172. In the bound form, Glu172 becomes positioned such that it can abstract an H atom from C2 of the substrate (Figs. 4*b*, 4*c* and 4*d*). After hydrogen abstraction, hydrogen bonding to Lys12 and His100 appears to form an oxyanion hole for the O2 atom of the enolate intermediate. His100 is also seen to hydrogen bond to O1 of the enolate in addition to O2. This shared hydrogen bonding is also seen in TIM NE2 (His95; Wierenga *et al.*, 2010). Comparison of the MtTPI–APO and MtTPI–GOL structures also reveals three conserved waters in the chain *A* active site (Figs. 4*b* and *d*). However, the MtTPI–PGH structure does not contain any of these molecules, indicating a possible entropic component to the binding of substrate.

To gain an insight into the kinetic parameters of the conversion of DHAP to D-GAP by MtTPI, the K_m and k_{cat} were determined enzymatically. The K_m was determined to be 2.5 ± 0.18 μ*M*. The k_{cat} of $4.38 \times 10^4 \pm 1.6 \times 10^3$ min^{-1} illustrates that MtTPI possibly spends minimal time in its DHAP substrate/product-bound form. Additionally, Mathur *et al.* (2006) determined the k_{cat} of the reverse reaction, conversion of D-GAP to DHAP, to be 4.1×10^6 min^{-1}, illustrating the preference of MtTPI for the D-GAP to DHAP reaction over its reverse. To explore the strength and thermodynamic nature of PGH binding, as well as to determine whether the absence of PGH in active site *B* might be a consequence of allosteric effects, the binding constant for PGH was determined using isothermal titration calorimetry (ITC). The dissociation constant of MtTPI–PGH was determined to be 7.28 ± 0.16 μ*M*, with a ΔH of -38.2 ± 0.1 kJ mol^{-1}, a ΔS of -226.5 ± 0.1 J mol^{-1} K^{-1} and an *n* value

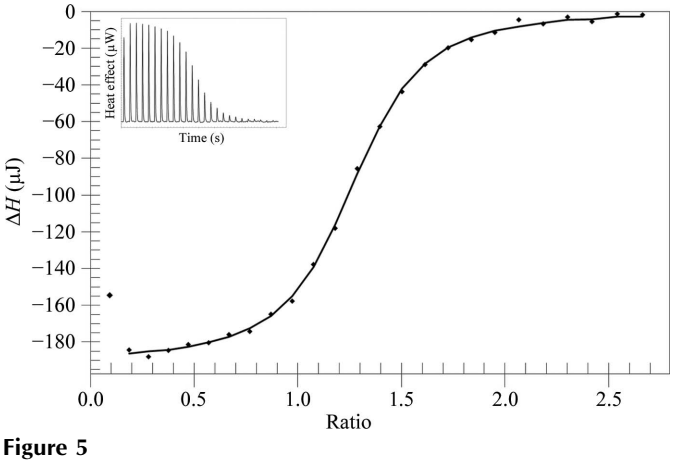

Figure 5
Calorimetric titration of MtTPI with PGH. Integrated heat peak areas are plotted against the molar ratio of PGH added to MtTPI. The last five data points were averaged for the heat of dilution and subtracted from the rest of the data. The line shows the best fit to an independent model $n = 1.24 \pm 0.01$, $K_d = 7.28 \pm 0.16$ μ*M*, $\Delta H = -38.2 \pm 0.1$ kJ mol^{-1} and $\Delta S = -226.5 \pm 0.1$ J mol^{-1} K^{-1}. The inset shows representative raw titration curves from 25 injections of 2.5 m*M* PGH into 170 µl MtTPI in 5 m*M* HEPES pH 7.4, 100 m*M* NaCl, 2 m*M* DTT at 298 K. This figure was generated using the *NanoAnalyze* software provided by TA Instruments.

equal to 1.24 ± 0.01. In contrast to the MtTPI–PGH structure, the ITC data show a 1:1 stoichiometry, indicating that both chains *A* and *B* bind PGH with an equal probability (Fig. 5).

4. Conclusion

Here, structures of MtTPI in its apo form and bound to the reaction-intermediate analog PGH are provided. Comparison of these structures with that of MtTPI–GOL suggests that the presence of glycerol reflects information on the apo form rather than substrate orientation within the MtTPI active site. However, in the presence of PGH a marked conformational change in the active site is observed, revealing how MtTPI may interact with and stabilize its reaction intermediates. Furthermore, the K_m and k_{cat} for the conversion of DHAP to D-GAP by MtTPI were revealed. As a result, elucidation of these structural changes lends insight into how substrates can bind to MtTPI.

This research was supported in part by the University of Denver's Partners in Scholarship (SEC) and Professional Research Opportunities for Faculty (SDP) programs as well as a grant from the Colorado Center for Drug Discovery (SDP). We thank Dr Olga Krasnykh from the Institute for Tuberculosis Research, the University of Illinois at Chicago for her gift of PGH. Data sets were collected on the Life Sciences Collaborative Access Team (LS-CAT) 21-ID-D beamline at the Advanced Photon Source, Argonne National Laboratory. Use of the Advanced Photon Source was supported by the US Department of Energy, Office of Science, Office of Basic Energy Sciences under Contract No. DE-AC02-06CH11357. Use of the LS-CAT Sector 21 for this project was supported by the Michigan Economic Development Corporation and the Michigan Technology Tri-Corridor (Grant 085P1000817).

References

Belasco, J. G., Herlihy, J. M. & Knowles, J. R. (1978). *Biochemistry*, **17**, 2971–2978.
Berlow, R. B., Igumenova, T. I. & Loria, J. P. (2007). *Biochemistry*, **46**, 6001–6010.
Davenport, R. C., Bash, P. A., Seaton, B. A., Karplus, M., Petsko, G. A. & Ringe, D. (1991). *Biochemistry*, **30**, 5821–5826.
Emsley, P. & Cowtan, K. (2004). *Acta Cryst.* D**60**, 2126–2132.
Gill, S. C. & von Hippel, P. H. (1989). *Anal. Biochem.* **182**, 319–326.
Kempf, J. G., Jung, J., Ragain, C., Sampson, N. S. & Loria, J. P. (2007). *J. Mol. Biol.* **368**, 131–149.
Mathur, D., Malik, G. & Garg, L. C. (2006). *FEMS Microbiol. Lett.* **263**, 229–235.
McCoy, A. J., Grosse-Kunstleve, R. W., Adams, P. D., Winn, M. D., Storoni, L. C. & Read, R. J. (2007). *J. Appl. Cryst.* **40**, 658–674.
Otwinowski, Z. & Minor, W. (1997). *Methods Enzymol.* **276**, 307–326.
Pegan, S. D., Rukseree, K., Franzblau, S. G. & Mesecar, A. D. (2009). *J. Mol. Biol.* **386**, 1038–1053.
Serratos, I. N., Pérez-Hernández, G., Garza-Ramos, G., Hernández-Arana, A., González-Mondragón, E. & Zubillaga, R. A. (2011). *J. Mol. Biol.* **405**, 158–172.
Wang, Y., Berlow, R. B. & Loria, J. P. (2009). *Biochemistry*, **48**, 4548–4556.
Wierenga, R. K. (2001). *FEBS Lett.* **492**, 193–198.
Wierenga, R. K., Kapetaniou, E. G. & Venkatesan, R. (2010). *Cell. Mol. Life Sci.* **67**, 3961–3982.
Winn, M. D. *et al.* (2011). *Acta Cryst.* D**67**, 235–242.
World Health Organization (2008). *The Global MDR-TB & XDR-TB Response Plan 2007–2008*, pp. 1–2. Geneva: World Health Organization.
World Health Organization (2010). *Global Tuberculosis Control 2010*, pp. 1–2. Geneva: World Health Organization.